Side-coupled resonators with parity-time symmetry for broadband unidirectional invisibility

Nicolas X. A. Rivolta* and Bjorn Maes
Micro- and Nanophotonic Materials Group, Faculty of Science, University of Mons, 20, Place du Parc, B-7000 Mons, Belgium
(Received 8 April 2016; published 28 November 2016)

We analyze the scattering properties of a parity-time ($\mathcal{PT}$)-symmetric structure made of a waveguide and a finite chain of side-coupled resonators. Typical one-dimensional $\mathcal{PT}$ structures exhibit unidirectional invisibility (also called anisotropic transmission resonances), meaning unity transmission and zero reflection for incidence from one direction. The side-coupled nature of our structure provides these features as well, but with different characteristics than the traditional tight-binding chain. We explore these properties in detail with numerical and analytical approaches for various chain lengths and geometries. As an interesting feature, we can achieve a broadband unidirectional invisibility with only two resonators. Furthermore, we observe rich dispersions for these anisotropic transmission resonances with four resonators, which can be carefully tuned.

DOI: 10.1103/PhysRevA.94.053854

I. INTRODUCTION

Originating from the fundamental studies of parity-time ($\mathcal{PT}$)-symmetric Hamiltonians in quantum mechanics [1,2], $\mathcal{PT}$-symmetric photonic structures have now been investigated for about a decade, as they combine gain and loss to achieve particular properties [3–6]. In optics loss is usually an unwanted feature that limits efficiency, but in the framework of $\mathcal{PT}$ symmetry it becomes a key element.

The balance between gain and loss typically indicates that the refractive index has to satisfy the symmetry relation $n(x) = n^*(-x)$, and in this context many optical devices have been revisited, such as the traditional directional coupler [7–12], switching devices [13,14], plasmonic structures [15], Bragg reflectors [16–19], microring resonators and microdisks [20–23], gratings [24–29], and others [30–39]. One of the most salient properties of these structures is spontaneous symmetry breaking at a certain loss and gain level, marking a clear transition via a so-called exceptional point between two phases with very different behavior.

We study the various effects of $\mathcal{PT}$ symmetry in a finite chain of resonators next to a waveguide (see Fig. 1). Because our geometry is side coupled, the behavior is very different from typical tight-binding or Bragg cavity structures [24,27]. A different side-coupled structure has very recently been explored in a $\mathcal{PT}$ context for sensor applications [40]. Our system can also be integrated on-chip, with independent control of the coupling loss (as it is an open system) and the material gain and loss. We use numerical and analytical calculations with coupled-mode theory in a transfer- and scattering-matrix approach to analyze in detail various geometries with multiple cavities.

We particularly focus on another important behavior of one-dimensional $\mathcal{PT}$ structures, the anisotropic transmission resonances (ATRs) [41] or unidirectional invisibility [42,43]. This means that one obtains unity transmission and zero reflection for incidence from one side, and a different reflection from the other side. In addition, we address the stability of these systems, as the presence of gain can readily make them unstable. Moreover, study of the scattering matrix provides us detailed information on exceptional points and on lasing states.

An important parameter for these coherently interacting cavities is the length of the intermediate waveguide, which can be tuned to change the phase and interference properties. The spectrum of two side-coupled resonators (without gain or loss) can exhibit a very narrow transmission peak [44,45]. We will exploit this peak with $\mathcal{PT}$ symmetry to demonstrate both very narrow and broadband ATRs.

For a chain of four resonators the possible configurations are even more numerous, as we can choose between a gain-gain-loss-loss or gain-loss-gain-loss profile, and we can even symmetrically modify the resonance frequencies and the amount of gain and loss, all the while remaining $\mathcal{PT}$ symmetric. We show that these configurations give rise to a unidirectional invisibility scheme with complex behavior as a function of the frequencies: a rich, tunable dispersion with multiple, crossing ATRs is obtained, offering possibilities for "ATR engineering."

We describe the two resonator structure in Sec. II and its scattering properties in Sec. II A. We study the lasing states and exceptional points in Sec. II B, and analyze the stability in Sec. II C. We show the versatility of these systems with a four resonator structure in Sec. III before concluding in Sec. IV.

II. TWO CAVITIES

The first structure is constituted of two resonators coupled next to a waveguide (see Fig. 1). We assume that the resonators and waveguide are single mode in the studied frequency region. Furthermore, the resonators are placed sufficiently far from each other so interaction occurs only through the waveguide. Then, the fields in a single unit cell can be described by coupled-mode theory [46]:

$$\frac{da_n}{dt} = \left(j\omega_0 - \frac{1}{\tau_c} \pm \gamma\right)a_n + df_n + db_{n+1}, \tag{1}$$

$$f_{n+1} = e^{j\phi} f_n + da_n, \tag{2}$$

$$b_n = e^{j\phi} b_{n+1} + da_n \tag{3}$$

with a_n the complex mode amplitude of the cavity, whereas f_n and f_{n+1} (b_n and b_{n+1}) denote the forward (backward)

*nicolas.rivolta@umons.ac.be

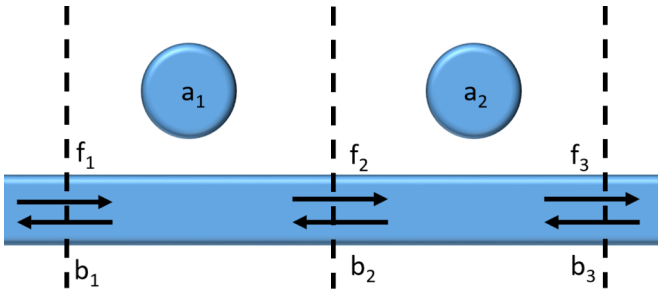

FIG. 1. Geometry of the two resonator structure. a_1 and a_2 are the mode amplitudes of each resonator. f_i (b_i) denotes the forward (backward) waveguide mode amplitude. The dashed lines separate the two unit cells of the system.

waveguide mode amplitudes, and $n = 1,2$. The coupling time to the waveguide is τ_c, and the resonance frequency of the cavities is ω_0. Here $d = je^{j\phi/2}/\sqrt{\tau_c}$, where ϕ depends on the length of the intermediate waveguide and plays a major role in the phase and interference characteristics. Finally, when $\gamma > 0$ it defines the amount of gain ($+\gamma$) or loss ($-\gamma$) present in the nth resonator, and vice versa when $\gamma < 0$. We mean here inherent gain or loss of the resonator via, e.g., external pumping of a gain medium, or material absorption. For a two resonator structure $\mathcal{PT}$ symmetry requires that one cavity supports gain and the other loss. The amplitudes are normalized so that $|a_n|^2$ is equal to the total power in the resonator n, and $|f_n|^2$ ($|b_n|^2$) is the power in the forward (backward) mode of the waveguide at position n. As we mainly work in the continuous-wave regime, the temporal dependence of the solution is $e^{j\omega t}$ and we can replace the time derivative d/dt by $j\omega$ with ω the excitation frequency and j the imaginary unit. In this side-coupling scheme, without gain or loss, there is a strong reflection on resonance. Note that these equations are equivalent to a model of a ring resonator next to two waveguides [47].

A. Reflection and transmission

We first examine the asymmetric reflection properties. A direct transfer-matrix approach is employed, which is much more resource efficient than a time domain one, but is insensitive to the stability (stability is studied in Sec. II C). The transfer matrix for one cavity can be written as

$$\begin{pmatrix} b_n \\ f_n \end{pmatrix} = \begin{pmatrix} e^{j\phi} - \frac{d^2}{j(\omega_0-\omega)\pm\gamma} & \frac{-d^2 e^{-j\phi}}{j(\omega_0-\omega)\pm\gamma} \\ \frac{d^2 e^{-j\phi}}{j(\omega_0-\omega)\pm\gamma} & e^{-j\phi} + \frac{d^2 e^{2j\phi}}{j(\omega_0-\omega)\pm\gamma} \end{pmatrix} \begin{pmatrix} b_{n+1} \\ f_{n+1} \end{pmatrix} = M_{\pm} \begin{pmatrix} b_{n+1} \\ f_{n+1} \end{pmatrix}. \quad (4)$$

The transfer matrix for the entire system M_{tot} is obtained by multiplication. As our scattering system is $\mathcal{PT}$ symmetric, we can use the formalism of [41] and define the total transfer matrix as a function of three real parameters (B and the phase and amplitude of A) via

$$M_{\text{tot}} = M_- M_+ = \begin{pmatrix} A^* & jB \\ -jC & A \end{pmatrix} \quad (5)$$

with C given by $C = (|A|^2 - 1)/B$ and M_- (M_+) denotes the transfer matrix for the cavity with loss (gain). Finally, we can

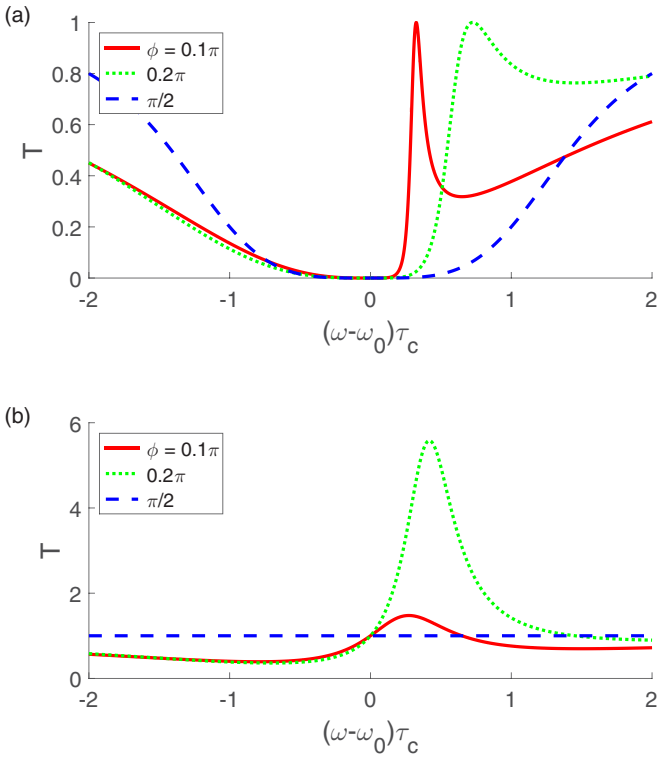

FIG. 2. Transmission of the two resonator structure as a function of the detuning $(\omega - \omega_0)\tau_c$ with three different values of ϕ, (a) for $\gamma\tau_c = 0$ and (b) for $\gamma\tau_c = 1$.

obtain the scattering matrix from the total transfer matrix:

$$S = \frac{1}{A}\begin{pmatrix} jB & 1 \\ 1 & jC \end{pmatrix} = \begin{pmatrix} r_L & t_c \\ t_c & r_R \end{pmatrix}, \quad (6)$$

with r_L and r_R the left and right reflection coefficient and t_c the transmission coefficient. This matrix is $\mathcal{PT}$ symmetric for our particular system [Eq. (4) and on], meaning that S satisfies the symmetry relation $(\mathcal{PT})S(\omega^*)(\mathcal{PT}) = S^{-1}(\omega)$ with $\mathcal{P} = \left(\begin{smallmatrix} 0 & 1 \\ 1 & 0 \end{smallmatrix}\right)$ and $\mathcal{T}$ the complex conjugation operator. From S we can extract all the information, such as the reflection with input from the left side $R_L = |r_L|^2$, the reflection from the right side $R_R = |r_R|^2$, and the transmission $T = |t_c|^2$. The transmission is the same regardless of the input side because of reciprocity.

We calculate the transmission for a loss-gain structure as a function of the normalized frequency detuning $(\omega - \omega_0)\tau_c$ (see Fig. 2). We observe the typical spectrum of two side-coupled resonators for three different phases ϕ with the normalized gain and loss factor $\gamma\tau_c = 0$ [without gain or loss, Fig. 2(a)]. The transmission reaches zero (and reflection reaches unity) at the resonance frequency ω_0. In addition, due to the cavity interaction, there is a narrow transmission peak (reaching $T = 1$) for small values of ϕ in the high reflection band. This peak becomes narrower and closer to $\omega = \omega_0$ as ϕ tends to zero. As we will see, the ATRs of these structures will directly originate from the extension of this particular peak for $\gamma\tau_c \neq 0$.

When $\gamma\tau_c$ is equal to 1 [Fig. 2(b)], the zero transmission zone around ω_0 tends to disappear. However, information about the ATRs necessitates the examination of the left and right side reflection, as they are no longer the same for $\gamma\tau_c \neq 0$.

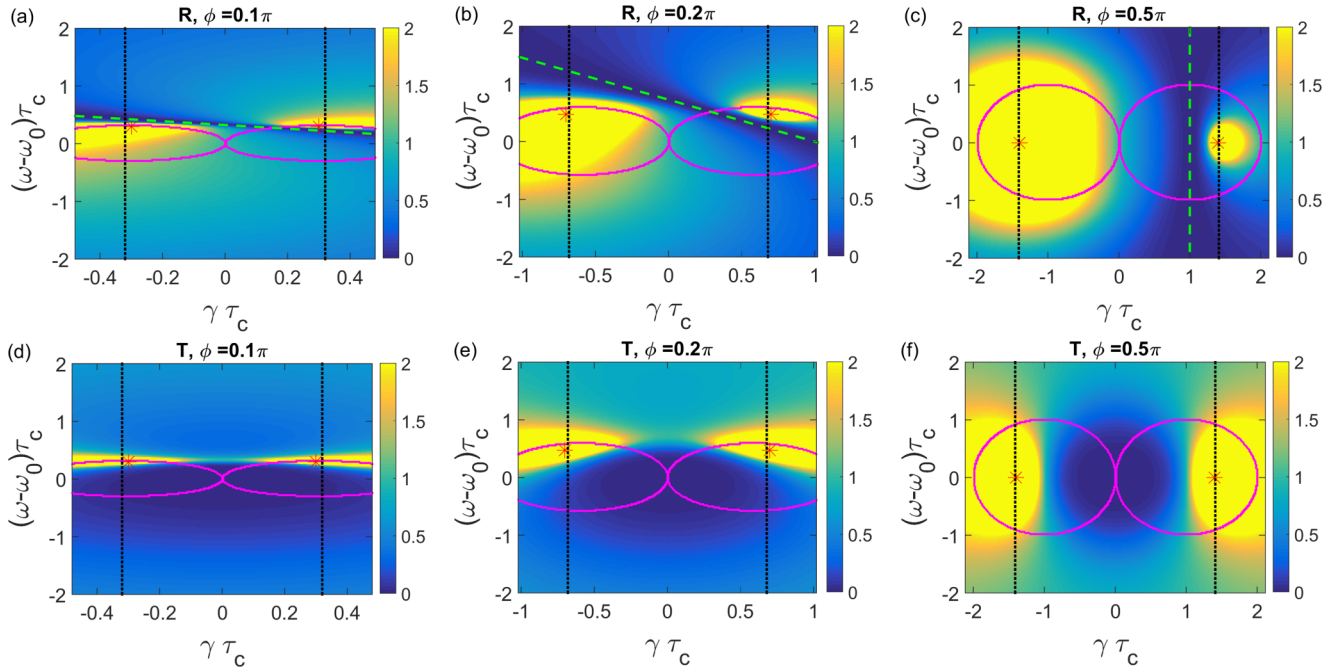

FIG. 3. Reflection (top row) and transmission (bottom row) for the two resonator structure (loss-gain) as a function of $\gamma\tau_c$ and detuning $(\omega-\omega_0)\tau_c$, and saturated to two for clarity. (a), (d) For $\phi = 0.1\pi$, (b), (e) for 0.2π, and (c), (f) for $\pi/2$. $\gamma\tau_c > 0$ (< 0) is for left (right) incidence. The green dashed lines represent the ATRs. The vertical black dotted lines represent the stability limit. The red stars indicate the lasing states and the magenta elliptical curves represent the exceptional points (Sec. II B).

Therefore we analyze the left and right reflection R together with the transmission T as a function of the detuning and $\gamma\tau_c$ for a loss-gain structure (Fig. 3). In these figures, left and right incidence corresponds to $\gamma\tau_c > 0$ and < 0, respectively (the right and left halves of the graphs).

The range $0 < \phi \leqslant \pi/2$ already presents all behaviors. The vertical black dotted lines indicate the maximum $\gamma\tau_c$ for stability, which is discussed in Sec. II C. Note that the transmission remains symmetric, and the graphs for $\gamma\tau_c > 0$ and < 0 are the same. However, the asymmetry between the left and right reflection is present for every value of ϕ. The ATRs arise when the reflection from a specific side reaches zero [dark blue zones in Figs. 3(a)–3(c), indicated with green dashed lines].

Interestingly, for fixed $\gamma\tau_c$, the sharpness of the zero reflection minimum is narrower as ϕ decreases. Thus, the frequency range of the ATRs is wider when ϕ increases, and becomes very broadband for $\phi = \pi/2$ [see Fig. 3(c)], which will be limited in practice by effects such as waveguide and material dispersion. This behavior is in line with the transmission resonances observed for $\gamma\tau_c = 0$ [Fig. 2(a)]. Note also that R and T are symmetric around $\omega = \omega_0$ for the special case of $\phi = \pi/2$.

ATRs arise when $T = 1$ [41], so with $|t_c|^2 = |1/A|^2 = 1$ we find an analytical condition for ATRs in this system:

$$(\omega - \omega_0)\tau_c = (1 - \tau_c\gamma)\tan\phi, \tag{7}$$

which is the equation of a straight line (green dashed lines in Fig. 3). This line is anchored at the point $\omega = \omega_0$ and $\gamma\tau_c = 1$ and has a slope of $-\tau_c\tan\phi$. Therefore with $\phi = \pi/2$ the slope indeed becomes infinite and we observe the broadband ATR of Fig. 3(c).

As T is symmetric around $\gamma\tau_c = 0$, one finds another line where $T = 1$, symmetric to the previously indicated ATR lines (dashed green lines). This line indicates the ATRs if we had chosen a gain-loss structure, instead of loss-gain, so this is not a "different" ATR. In that case, R should be mirrored in Fig. 3.

Finally, we also observe that there tends to be more reflection when incidence is from the gain side than from the loss side, as indeed the yellow zones are larger on the left of Figs. 3(a)–3(c).

We conclude that the two resonator system already presents a fairly complex behavior of asymmetric scattering properties, deriving from the passive transmission resonances. The geometry can achieve both very narrow and broadband ATRs just by varying the length of the intermediate waveguide.

We remark that the model neglects some effects that can influence the results for specific applications and intensities. First, dispersion will ultimately limit the broadband ATRs to a finite range of frequencies. For waveguide dispersion the geometry and materials could offer degrees of freedom to optimize the available range, for example, with photonic crystal waveguide engineering. Material dispersion will also impact the ATR range, certainly via the finite window of active materials. We also note that the complex permittivity of the materials will follow the Kramers-Kronig relations, which can distort the characteristics. Second, gain saturation and charge-carrier dynamics in the gain material will limit the maximal $\gamma\tau_c$ that can be reached in practice. Third, the large intensities around the lasing states will break the linear approximation, and may lead to new carrier and nonlinear effects, temporal instabilities [48], switching behavior, and so on. The latter phenomena are expected mainly around the

stability threshold, so below the gain values for the discussed ATRs.

B. Lasing states and exceptional points

Another interesting feature of active structures is the lasing states that can arise from the presence of gain. These states can be derived from the scattering matrix [Eq. (6)], as T, R_L, and R_R become infinite when $A = 0$, leading to

$$(\omega - \omega_0)\tau_c = -j(1 + e^{-j\phi}\sqrt{e^{2j\phi}\tau_c^2\gamma^2 + 1}). \tag{8}$$

Lasing states require a purely real frequency. Therefore the left side of this equation has to be purely real, so the lasing states exist only when the imaginary part of the right side is equal to zero, which we indicate with red stars in Fig. 3. Within the numerical accuracy these points are at the stability limit (vertical black dotted lines in Fig. 3, discussed in detail in Sec. II C). The two cavity structure has two lasing states, but they are exactly at the same detuning and gain and loss, which is understandable as T is reciprocal, so there is left-right symmetry in Figs. 3(d)–3(f).

Furthermore, as the S matrix respects $\mathcal{PT}$ symmetry, there is a broken and an unbroken $\mathcal{PT}$ phase. In the unbroken phase each S-matrix eigenstate is mapped back to itself under the $\mathcal{PT}$ operation, whereas in the broken phase they are mapped to each other. At the boundary, called the exceptional points, the two eigenstates merge. To identify these phases one can examine the eigenvalues of S [41], which have unity module only in the unbroken phase. Alternatively, one can use the quantity $(R_L + R_R)/2 - T$, which is below (above) unity in the unbroken (broken) phase, respectively. When this quantity is equal to one, it describes the boundary between the two phases, shown as the magenta elliptical lines in Fig. 3. We observe that the lasing states only appear in the broken phase (inside the magenta lines) in accordance with [49].

Thus, as in other $\mathcal{PT}$ devices, the two side-coupled resonator structure presents lasing states and a broken $\mathcal{PT}$ phase. In our model the particular states are fairly straightforward to determine analytically.

C. Stability

The main advantage of this structure concerns the versatility of the scattering properties. However, a stationary transfer-matrix formalism fails to take into account a possible instability of the system, which is common in the presence of gain [50]. Therefore, we analyze the stability range, via the matrix H that describes the system without external excitation:

$$\frac{d}{dt}\begin{pmatrix} a_1 \\ a_2 \end{pmatrix} = H\begin{pmatrix} a_1 \\ a_2 \end{pmatrix} \tag{9}$$

with

$$H = \begin{pmatrix} j\omega_0 - 1/\tau_c - \gamma & d^2 \\ d^2 & j\omega_0 - 1/\tau_c + \gamma \end{pmatrix} \tag{10}$$

where the first resonator supports loss and the second supports gain ($\gamma > 0$ here). Unlike the S matrix, H is neither Hermitian nor $\mathcal{PT}$ symmetric due to the coupling with the waveguide. The energy contained in the resonators and the intermediate waveguide flows out of the system. The eigenvalues λ of H describe the evolution of the collective eigenstates:

$$\lambda_{1,2} = \left(j\omega_0 - \frac{1}{\tau_c}\right) \pm \sqrt{\gamma^2 + \frac{e^{2j\phi}}{\tau_c^2}}. \tag{11}$$

The imaginary part of these eigenvalues represents the eigenfrequency of the modes. The real part represents the time evolution of the total power inside the two cavity system.

We plot λ as a function of $\gamma\tau_c$ (Fig. 4) for three values of ϕ. Without gain or loss ($\gamma\tau_c = 0$), the two eigenvalues have a negative real part [see Figs. 4(a), 4(c), and 4(e)], which means that the total power present in the cavities is flowing out of the system through the waveguide.

Remark that even though we are not describing a pure $\mathcal{PT}$-symmetric structure here, we observe similar curve shapes, especially for $\phi = \pi/2$ [Figs. 4(e) and 4(f)]. The imaginary parts of the eigenvalues merge together, whereas the two real parts split beyond a particular point, which thus looks like an exceptional point (at $\gamma\tau_c = 1$). As ϕ decreases, this behavior looks less and less like "perfect" $\mathcal{PT}$, which is comparable to a directional $\mathcal{PT}$ coupler with unequal waveguides [Figs. 4(a)–4(d)].

For stability, we focus on the real part of the eigenvalues. When one is positive, it shows us that the power inside the cavities grows exponentially with time. When $\gamma\tau_c$ increases, one of the modes always reaches a point where its real part becomes positive [e.g., at $\gamma\tau_c \approx 0.7$ in Fig. 4(a)], leading to

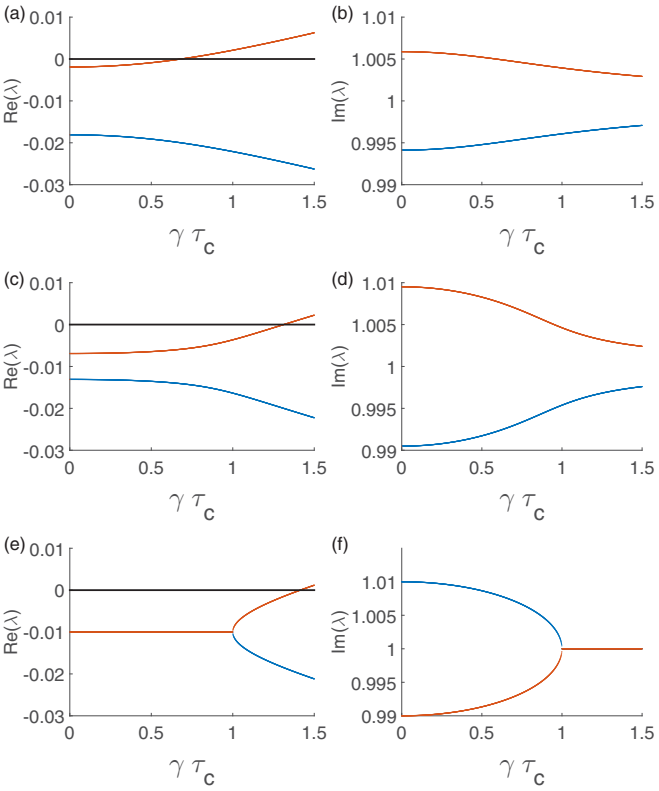

FIG. 4. Real (left column) and imaginary (right column) part of the eigenvalues $\lambda_{1,2}$ as a function of $\gamma\tau_c$ for (a), (b) $\phi = 0.2\pi$, (c), (d) 0.4π, and (e), (f) $\pi/2$. The black horizontal line in the left column marks $\mathrm{Re}(\lambda) = 0$, the instability threshold.

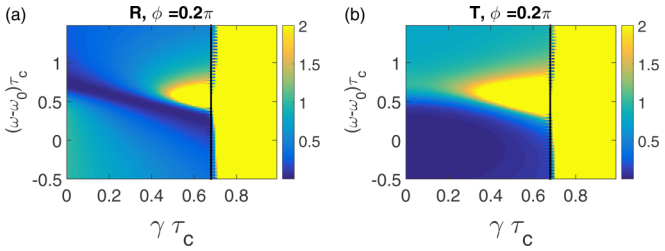

FIG. 5. (a) Left reflection and (b) transmission as a function of the detuning and $\gamma\tau_c$ for a loss-gain structure. The parameters are the same as in Fig. 2. These values are calculated with time domain simulations and are saturated to two for clarity. The black lines mark when one of the eigenvalues begins to have a positive real part [around $\gamma\tau_c \approx 0.7$ in Fig. 4(a)].

unstable behavior that ultimately will become nonlinear and requires other modeling approaches.

We check the previous with time domain simulations of R and T as a function of the detuning $(\omega-\omega_0)\tau_c$ and $\gamma\tau_c$ (see Fig. 5). The boundary between the stable and the unstable regime is well described by the zero of the real part of the eigenvalue (vertical black lines in Fig. 5), and corresponds with an exponential growth in the time domain results. Thus, for each configuration we can define a maximum limit for $\gamma\tau_c$ beyond which the system is unstable, defining a valid range of gain and loss.

III. FOUR CAVITIES

We further show the versatility of these systems with a four resonator geometry. We skip the three resonator system as it offers less degrees of freedom and behaviors. We use the same formalism as in the previous section. In principle most results can be analytically derived, but the equations become unwieldly, so calculations are more convenient.

The transmission T of a four resonator structure without loss and gain for four values of ϕ is shown in Fig. 6. Typically there are three peaks with $T=1$ (and $R=0$) for four resonators. For $\phi=0.1\pi$ the three peaks are relatively close to each other around $\omega_0=\omega$. When ϕ increases the three peaks move to the right, and the rightmost peak (number 3) tends to infinite detuning when ϕ reaches $\pi/4$. Beyond this

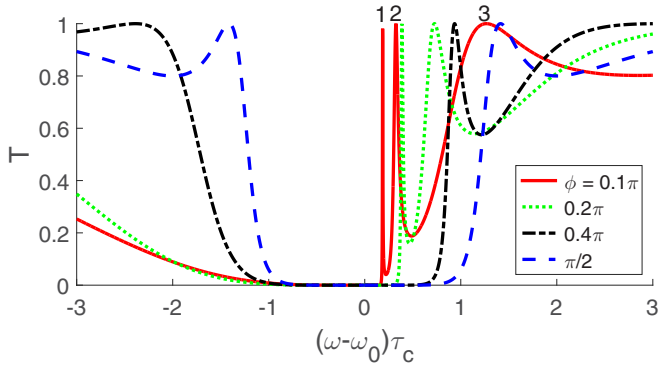

FIG. 6. Transmission of the four resonator structure as a function of the detuning $(\omega-\omega_0)\tau_c$ for $\gamma\tau_c=0$ with four different values of ϕ. The three numbers indicate the three peaks with $T=1$ for $\phi=0.1\pi$.

value of ϕ peak 3 appears from minus infinity and continues moving to the right. Finally, when ϕ reaches $\pi/2$, peak 2 also moves to infinite detuning. This pattern continues as ϕ increases. As previously the ATRs of the $\mathcal{PT}$-symmetric system will originate from the behaviors of these three peaks.

We calculate the reflection and transmission with a loss-gain-loss-gain profile for three phases (Fig. 7). We observe two kinds of ATRs. There is a straight line ATR where the reflection is zero [slanted green line in Figs. 7(a)–7(c)], but for only one incidence direction. This line originates from the second peak with $T=1$ in Fig. 6 and can be compared to the ATR line of the two resonator structure [green dashed line in Figs. 3(a)–3(c)]. This ATR becomes very broadband [Fig. 7(c)] when peak 2 goes to infinite detuning.

Additionally, there is an ATR where $R_R=R_L=0$ and $T=1$, which originates from peaks 1 and 3 [nearly horizontal green line in Fig. 7(a) and green ellipse in Figs. 7(b) and 7(c)]. This indicates a "doubly accidental" degeneracy [41] where both reflections are equal to zero, so the structure is transparent from both directions. This can appear due to extra tuning parameters, but seems inherent in our geometry. The latter type of ATR would actually better be described as an "isotropic" transmission resonance. We can observe that the ellipse becomes infinitely large [Fig. 7(a)] as peak 3 goes to infinity (for $\phi=\pi/4$), so we only observe a horizontal line close to $(\omega-\omega_0)\tau_c=0.5$.

The structure also exhibits two lasing states at the limit of the stable range. There are two additional lasing states but they lie deeper into the unstable part. The exceptional point boundaries are also more complicated, with four zones instead of two for the two resonator structure (magenta curves in Fig. 7). As in Fig. 3, we observe that the reflection tends to be stronger when the incidence is from the gain side (larger yellow areas on the left side of R).

The degrees of liberty for this structure are numerous as we are only limited by the $\mathcal{PT}$-symmetry relation $n(x)=n^*(-x)$. For example, if we change the elements symmetrically, we can vary the gain and loss profile (such as loss-loss-gain-gain instead of loss-gain-loss-gain), the resonance frequencies of the cavities (ω_1 has to equal ω_4, and ω_2 has to equal ω_3, but the couples can differ), the amount of gain and loss in the cavities, and the phase ϕ. We describe succinctly a few examples (Fig. 8) where we observe rich possibilities for the ATRs, the exceptional points, and the lasing states.

As a first example, we examine a loss-loss-gain-gain profile, in contrast with the previous loss-gain-loss-gain design. The reflection graph with ATRs and exceptional points is qualitatively different [Fig. 8(a)], with, for example, two pairs of lasing states, in contrast with the single pair in Fig. 7 [and in particular with Fig. 7(c) for the same phase].

In the other examples we return to a loss-gain-loss-gain profile, but we change the gain and loss values. In Fig. 8(b) with a gain and loss sequence $(-0.3\gamma,\gamma,-\gamma,0.3\gamma)$, we observe an interaction between the line and ellipse of ATRs of Fig. 7(b), which looks similar to "anticrossing" behavior. In Fig. 8(c) the structure has a gain and loss sequence $(-0.01\gamma,\gamma,-\gamma,0.01\gamma)$ leading to another qualitative change of the ATRs, specifically the elliptical ATR of Fig. 7(c) becomes a parabola in Fig. 8(c). Furthermore, the change of the exceptional points is even more complicated.

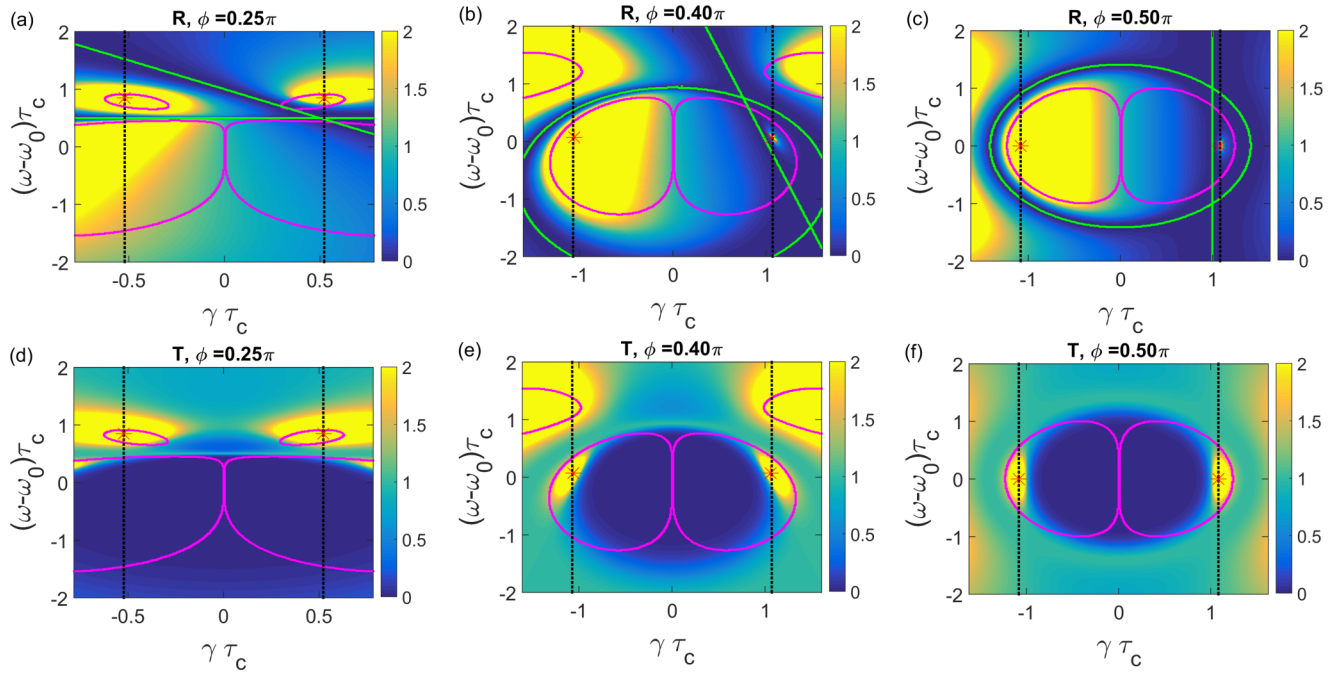

FIG. 7. Reflection (top row) and transmission (bottom row) for four resonators (loss-gain-loss-gain) as a function of $\gamma\tau_c$ and the detuning $(\omega-\omega_0)\tau_c$, and saturated to two for clarity. (a), (d) For $\phi=\pi/4$, for (b), (e) 0.4π, and for (c), (f) $\pi/2$. $\gamma\tau_c>0$ (<0) is the reflection and transmission for left (right) incidence. The black dotted lines represent the stability limit. The green lines show the ATRs, the red stars indicate the laser states, and the magenta curves represent the limits of the broken-symmetry phase.

As another example we change the resonance frequencies, while keeping $\mathcal{PT}$ symmetry. For Fig. 8(d) we use the frequencies $(\omega_0,\omega_0-1/\tau_c,\omega_0-1/\tau_c,\omega_0)$, but with the standard gain and loss $(-\gamma,\gamma,-\gamma,\gamma)$. We observe a very flat and narrow ATR, similar to the nearly horizontal ATR of Fig. 7(a). But here the reflection is zero for only one incidence direction [the

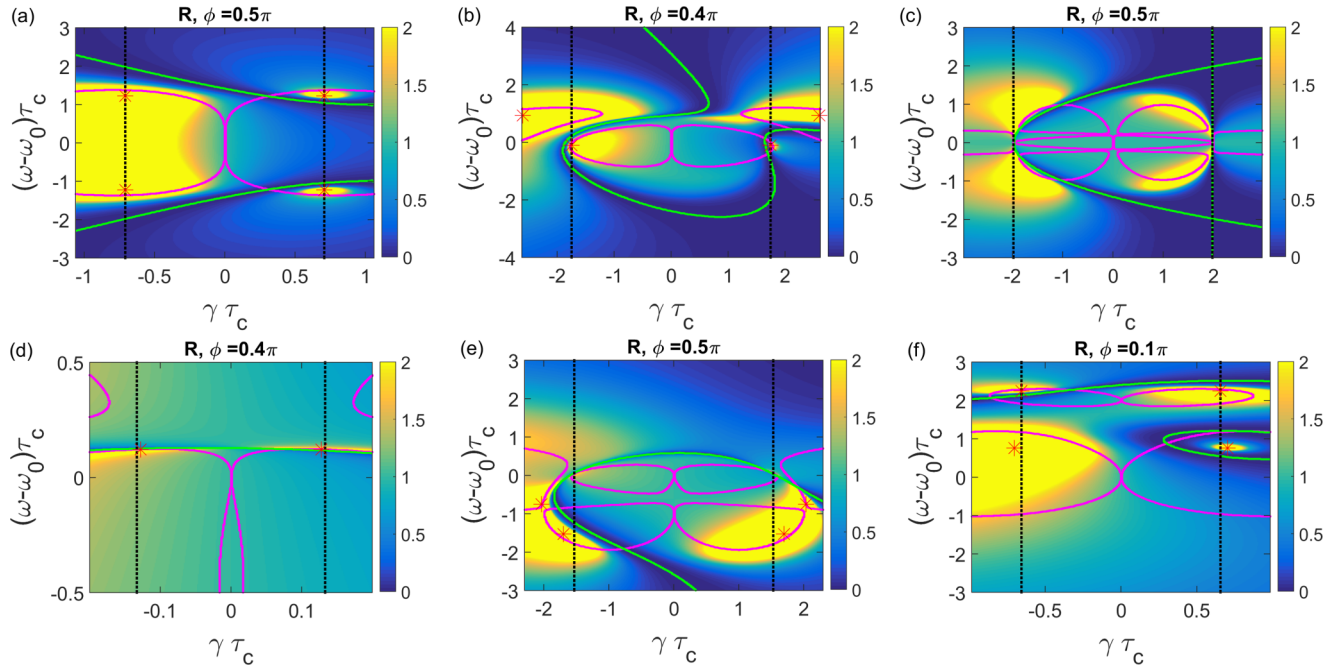

FIG. 8. Reflection for various four resonator structures as a function of $\gamma\tau_c$ and the detuning $(\omega-\omega_0)\tau_c$, and saturated to two for clarity. (a) Loss-loss-gain-gain structure with resonance frequency sequence $(\omega_0,\omega_0,\omega_0,\omega_0)$ and gain and loss sequence $(-\gamma,-\gamma,\gamma,\gamma)$. The other structures are loss-gain-loss-gain with sequences (b) $(\omega_0,\omega_0,\omega_0,\omega_0)$ and $(-0.3\gamma,\gamma,-\gamma,0.3\gamma)$, (c) $(\omega_0,\omega_0,\omega_0,\omega_0)$ and $(-0.01\gamma,\gamma,-\gamma,0.01\gamma)$, (d) $(\omega_0,\omega_0-1/\tau_c,\omega_0-1/\tau_c,\omega_0)$ and $(-\gamma,\gamma,-\gamma,\gamma)$, (e) $(\omega_0,\omega_0-1/\tau_c,\omega_0-1/\tau_c,\omega_0)$ and $(-0.1\gamma,\gamma,-\gamma,0.1\gamma)$, and (f) $(\omega_0,\omega_0+2/\tau_c,\omega_0+2/\tau_c,\omega_0)$ and $(-\gamma,0.5\gamma,-0.5\gamma,\gamma)$. Vertical black dotted lines are stability limits, green lines are ATRs, red stars are lasing states, and magenta lines indicate exceptional points.

green curve is very slightly slanted in Fig. 8(d)], and we are not in the doubly accidental degeneracy case of Fig. 7(a).

For the final examples we change both resonance frequency and gain and loss sequences. For Fig. 7(e) we use the frequencies $(\omega_0,\omega_0-1/\tau_c,\omega_0-1/\tau_c,\omega_0)$ and the gain and loss sequence $(-0.1\gamma,\gamma,-\gamma,0.1\gamma)$. We observe a similar interaction between the ATR line and ellipse as in Fig. 8(b), but mirrored as a function of detuning. In comparison, there are also two more broken-symmetry zones. Finally, Fig. 8(f) with $(\omega_0,\omega_0+2/\tau_c,\omega_0+2/\tau_c,\omega_0)$ and $(-\gamma,0.5\gamma,-0.5\gamma,\gamma)$ shows another behavior, and can barely be compared to previous cases.

One observes that the number of possible configurations and behaviors quickly grows with the number of cavities. Thus a particular desired behavior can be targeted via the analytical model for a relatively small number of cavities.

IV. CONCLUSION

We introduce a $\mathcal{PT}$ geometry consisting of side-coupled cavities with interesting unidirectional characteristics. In these systems we show that the bandwidth can be uniquely tuned to be particularly broad or narrow, via a simple structural parameter (the length of the waveguide between the cavities). The unidirectional effect is one of the most salient features in the $\mathcal{PT}$ field; it is strongly researched nowadays for potential applications. The proposed design can be implemented on-chip in various ways, for example, using photonic crystal cavities or ring resonators.

With a compact, physical model we have analyzed in detail the scattering characteristics of the one-dimensional structures with side-coupled resonators. Because of side coupling the behavior is very different from typical tight-binding or Bragg defect structures. It is also an analytically tractable open system with flexible control of cavity-waveguide coupling and the intrinsic gain and loss.

The spectrum of two resonators (without gain or loss) exhibits a very narrow transmission ($R=0$) peak. With added gain and loss the ATRs originate precisely from this peak, which can be tuned by the length of the intermediate waveguide, in order to demonstrate very narrow or broadband ATRs. Moreover, the study of the scattering matrix provides us detailed information on related important properties, such as the lasing states, the exceptional points, and the stability of the system.

Furthermore, the versatility of these systems is exhibited with a chain of four resonators. The possible degrees of freedom are numerous, as we can choose between a gain-gain-loss-loss or gain-loss-gain-loss profile, and we can even symmetrically modify the frequencies of the resonators and the amount of gain and loss. Each of these configurations gives rise to a unidirectional (or bidirectional) invisibility scheme with complex behavior as a function of the frequencies: a rich, tunable dispersion with multiple, crossing, or anticrossing ATRs is obtained, offering possibilities for "ATR engineering."

In future work one could also explore structures without perfect $\mathcal{PT}$ geometry, with, e.g., gain and loss profiles that are not left-right symmetric. These would often lead to imperfect ATRs, however, with reflections that are not perfectly zero. We do not explore these cases here, but they would significantly expand the available parameter space.

ACKNOWLEDGMENTS

This work is supported by the Belgian Science Policy Office under the project "Photonics@be" (P7-35) and by the Fonds National de Recherche Scientifique in Belgium.

[1] C. M. Bender and S. Boettcher, Phys. Rev. Lett. **80**, 5243 (1998).
[2] C. M. Bender, Rep. Prog. Phys. **70**, 947 (2007).
[3] A. Guo, G. J. Salamo, D. Duchesne, R. Morandotti, M. Volatier-Ravat, V. Aimez, G. A. Siviloglou, and D. N. Christodoulides, Phys. Rev. Lett. **103**, 093902 (2009).
[4] L. Razzari and R. Morandotti, Nature (London) **488**, 163 (2012).
[5] A. Lupu, H. Benisty, and A. Degiron, Opt. Express **21**, 21651 (2013).
[6] H. Ramezani, T. Kottos, R. El-Ganainy, and D. N. Christodoulides, Phys. Rev. A **82**, 043803 (2010).
[7] N. X. A. Rivolta and B. Maes, Opt. Lett. **40**, 3922 (2015).
[8] C. E. Ruter, K. G. Makris, R. El-Ganainy, D. N. Christodoulides, M. Segev, and D. Kip, Nat. Phys. **6**, 192 (2010).
[9] R. El-Ganainy, K. G. Makris, D. N. Christodoulides, and Z. H. Musslimani, Opt. Lett. **32**, 2632 (2007).
[10] S. Klaiman, U. Günther, and N. Moiseyev, Phys. Rev. Lett. **101**, 080402 (2008).
[11] J. Čtyroký, V. Kuzmiak, and S. Eyderman, Opt. Express **18**, 21585 (2010).
[12] S. V. Suchkov, S. V. Dmitriev, B. A. Malomed, and Y. S. Kivshar, Phys. Rev. A **85**, 033825 (2012).
[13] N. X. A. Rivolta and B. Maes, J. Opt. Soc. Am. B **32**, 1330 (2015).
[14] S. Phang, A. Vukovic, H. Susanto, T. M. Benson, and P. Sewell, J. Opt. Soc. Am. B **30**, 2984 (2013).
[15] H. Benisty, A. Degiron, A. Lupu, A. D. Lustrac, S. Chénais, S. Forget, M. Besbes, G. Barbillon, A. Bruyant, S. Blaize, and G. Lérondel, Opt. Express **19**, 18004 (2011).
[16] M. Kulishov, J. Laniel, N. Bélanger, J. Azaña, and D. Plant, Opt. Express **13**, 3068 (2005).
[17] A. Mostafazadeh, Phys. Rev. Lett. **102**, 220402 (2009).
[18] M. Kulishov and B. Kress, Opt. Express **21**, 22327 (2013).
[19] M. Kulishov and B. Kress, Opt. Express **20**, 29319 (2012).
[20] L. Feng, Z. J. Wong, R.-M. Ma, Y. Wang, and X. Zhang, Science **346**, 972 (2014).
[21] B. Peng, S. K. Özdemir, F. Lei, F. Monifi, M. Gianfreda, G. L. Long, S. Fan, F. Nori, C. M. Bender, and L. Yang, Nat. Phys. **10**, 394 (2014).
[22] B. Peng, S. K. Özdemir, S. Rotter, H. Yilmaz, M. Liertzer, F. Monifi, C. M. Bender, F. Nori, and L. Yang, Science **346**, 328 (2014).
[23] M. Brandstetter, M. Liertzer, C. Deutsch, P. Klang, J. Schöberl, H. E. Türeci, G. Strasser, K. Unterrainer, and S. Rotter, Nat. Commun. **5**, 4034 (2014).
[24] H. Ramezani, D. N. Christodoulides, V. Kovanis, I. Vitebskiy, and T. Kottos, Phys. Rev. Lett. **109**, 033902 (2012).

[25] A. Regensburger, C. Bersch, M.-A. Miri, G. Onishchukov, D. N. Christodoulides, and U. Peschel, Nature (London) **488**, 167 (2012).
[26] K. G. Makris, R. El-Ganainy, D. N. Christodoulides, and Z. H. Musslimani, Phys. Rev. A **81**, 063807 (2010).
[27] M. C. Zheng, D. N. Christodoulides, R. Fleischmann, and T. Kottos, Phys. Rev. A **82**, 010103 (2010).
[28] K. G. Makris, R. El-Ganainy, D. N. Christodoulides, and Z. H. Musslimani, Phys. Rev. Lett. **100**, 103904 (2008).
[29] R. Uzdin and N. Moiseyev, Phys. Rev. A **85**, 031804 (2012).
[30] S. Phang, A. Vukovic, S. C. Creagh, P. D. Sewell, G. Gradoni, and T. M. Benson, Scientific Reports **6**, 20499 (2016).
[31] Y. D. Chong, L. Ge, and A. D. Stone, Phys. Rev. Lett. **106**, 093902 (2011).
[32] S. Savoia, G. Castaldi, V. Galdi, A. Alù, and N. Engheta, Phys. Rev. B **89**, 085105 (2014).
[33] G. Castaldi, S. Savoia, V. Galdi, A. Alù, and N. Engheta, Phys. Rev. Lett. **110**, 173901 (2013).
[34] C. He, M.-H. Lu, X. Heng, L. Feng, and Y.-F. Chen, Phys. Rev. B **83**, 075117 (2011).
[35] A. E. Miroshnichenko, B. A. Malomed, and Y. S. Kivshar, Phys. Rev. A **84**, 012123 (2011).
[36] S. Longhi, Phys. Rev. A **82**, 031801 (2010).
[37] M. Liertzer, L. Ge, A. Cerjan, A. D. Stone, H. E. Türeci, and S. Rotter, Phys. Rev. Lett. **108**, 173901 (2012).
[38] T. Kottos, Nat. Phys. **6**, 166 (2010).
[39] B. Zhu, R. Lu, and S. Chen, Phys. Rev. A **91**, 042131 (2015).
[40] J. Li, R. Yu, C. Ding, and Y. Wu, Phys. Rev. A **93**, 023814 (2016).
[41] L. Ge, Y. D. Chong, and A. D. Stone, Phys. Rev. A **85**, 023802 (2012).
[42] Z. Lin, H. Ramezani, T. Eichelkraut, T. Kottos, H. Cao, and D. N. Christodoulides, Phys. Rev. Lett. **106**, 213901 (2011).
[43] Y. Huang, G. Veronis, and C. Min, Opt. Express **23**, 29882 (2015).
[44] B. Maes, P. Bienstman, and R. Baets, J. Opt. Soc. Am. B **22**, 1778 (2005).
[45] B. Maes, M. Soljacic, J. D. Joannopoulos, P. Bienstman, R. Baets, S.-P. Gorza, and M. Haelterman, Opt. Express **14**, 10678 (2006).
[46] S. Fan, W. Suh, and J. D. Joannopoulos, J. Opt. Soc. Am. A **20**, 569 (2003).
[47] D. G. Rabus, *Integrated Ring Resonators* (Springer, New York, 2007).
[48] B. Maes, M. Fiers, and P. Bienstman, Phys. Rev. A **80**, 033805 (2009).
[49] P. Ambichl, K. G. Makris, L. Ge, Y. Chong, A. D. Stone, and S. Rotter, Phys. Rev. X **3**, 041030 (2013).
[50] X. Jiang, Q. Li, and C. M. Soukoulis, Phys. Rev. B **59**, R9007(R) (1999).